NANO LETTERS
Letter
Cite This: Nano Lett. 2019, 19, 1605−1612
pubs.acs.org/NanoLett

Thermal Spin Injection and Inverse Edelstein Effect of the Two-Dimensional Electron Gas at EuO−$KTaO_3$ Interfaces

Hongrui Zhang,[†,‡] Yang Ma,[§,∥] Hui Zhang,[†,‡] Xiaobing Chen,[†,‡] Shuanhu Wang,[⊥] Gang Li,[†,‡] Yu Yun,[§,∥] Xi Yan,[†,‡] Yuansha Chen,[†,‡] Fengxia Hu,[†,‡,#] Jianwang Cai,[†,‡] Baogen Shen,[†,‡,#] Wei Han,[§,∥] and Jirong Sun*[,†,‡,#]

[†]Beijing National Laboratory for Condensed Matter Physics & Institute of Physics, Chinese Academy of Sciences, Beijing 100190, People's Republic of China

[‡]School of Physics, University of the Chinese Academy of Sciences, Beijing 100049, People's Republic of China

[§]International Centre for Quantum Materials, School of Physics, Peking University, Beijing 100871, People's Republic of China

[∥]Collaborative Innovation Centre of Quantum Matter, Beijing 100871, People's Republic of China

[⊥]Shanxi Key Laboratory of Condensed Matter Structures and Properties, School of Science, Northwestern Polytechnic University, Xi'an 710072, People's Republic of China

[#]Songshan Lake Materials Laboratory, Dongguan, Guangdong 523808, People's Republic of China

Supporting Information

ABSTRACT: With the help of the two-dimensional electron gas (2DEG) at the $LaAlO_3$−$SrTiO_3$ interface, spin and charge currents can be interconverted. However, the conversion efficiency has been strongly depressed by $LaAlO_3$, which blocks spin transmission. It is therefore highly desired to explore 2DEGs sandwiched between ferromagnetic insulators that are transparent for magnons. By constructing epitaxial heterostructure with ferromagnetic EuO, which is conducting for spin current but insulating for electric current, and $KTaO_3$, we successfully obtained the 2DEGs, which can receive thermally injected spin current directly from EuO and convert the spin current to charge current via inverse Edelstein effect of the interface. Strong dependence of the spin Seebeck coefficient on the layer thickness of EuO is further observed and the propagation length for non-equilibrium magnons in EuO has been determined. The present work demonstrates the great potential of the 2DEGs formed by ferromagnetic oxides for spin caloritronics.

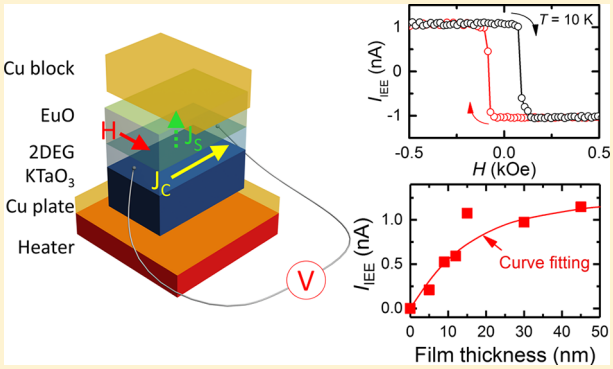

KEYWORDS: *2DEG, thermal spin injection, spin-charge conversion, inverse Edelstein effect, Rashba spin splitting*

The two-dimensional electron gases (2DEGs) confined to the heterointerfaces of two non-magnetic insulators $LaAlO_3$ (LAO) and $SrTiO_3$ (STO) have received intensive attention in the past decade because of their exotic properties that may lead to new conceptual physics and potential applications. Novel effects stemming from interfacial reconstruction have been observed, including 2D superconductivity and its coexistence with ferromagnetism,[1−4] abnormal increase in superconducting temperature with magnetic fields,[5] giant thermopower,[6] current-driven Rashba field,[7] out-of-plane spin texture,[8] strong gating effect on interfacial conductance,[9] etc.

Due to broken spatial inversion symmetry, the conducting interface owns a unique character, i.e., Rashba-type spin−orbit coupling. In addition to splitting energy band of the 2DEG according to spin texture, this distinct spin−orbit coupling causes a spin-momentum locking, i.e., electron spins align along a direction parallel to interface but perpendicular to electron momentum. Consequently, non-equilibrium spin accumulation will appear once an electric current is applied along interface, yielding an output of spin current. This is the so-called Edelstein effect (EE).[10] On the contrary, injecting spin current into interface will result in an inverse Edelstein effect (IEE), i.e., an electric current along interface.

Based on the technique of ferromagnetic resonance (FMR), the IEE has been intensively studied in the past few years by directly injecting spin current to the interfaces of metallic multilayers, including NiFe/Ag/Bi,[11] NiFe/Ag/Sb,[12] Fe/Ag/Sn,[13] NiFe/$Bi_{1.5}Sb_{0.5}Te_{1.7}Se_{1.3}$, and NiFe/Sn-doped Bi_2Te_2Se.[14] For conducting oxide interfaces, spin-to-charge conversion was also realized in recently years after pumping

Received: November 8, 2018
Revised: January 16, 2019
Published: February 4, 2019

DOI: 10.1021/acs.nanolett.8b04509
Nano Lett. 2019, 19, 1605−1612

spin current into the 2DEGs at the LAO−STO interfaces.[15,16] Different from the case of metallic multilayers, spin current now has to transmit through an insulating layer (LAO) to reach interface. Soon afterward, the EE was reported for the same kind of oxide interface.[17] It was found that a radio frequency current applied to the LAO−STO interface produced a spin current, causing a magnetic precession of the ferromagnetic (FM) cap layer. In particular, the spin−orbit torque efficiency is unprecedentedly high (~6.3 at room temperature), almost 2 orders of magnitude larger than the spin Hall angles in heavy metals such as Pt and Ta.

Among these works, the spin-charge conversion via the LAO−STO interface is of special interest because, in a sense, it reveals the great potential for spintronics of oxide interface with strong electron correlation and thus deserves further investigations. Unfortunately, the IEE (EE) of the LAO/STO system has been significantly depressed by the LAO layer, which impedes the transmission of spin current especially at low temperatures.[16] In addition to this, FMR spin pumping, which has been frequently adopted while investigating the physical processes associated with spin current, has drawbacks. Although it is powerful in generating strong spin current, as is well-documented,[18−21] sometimes it introduces parasitic effects that must be completely eliminated or else spurious signals will lead to a misunderstanding of the experimental results.[22] Therefore, it is highly desired to get new 2DEGs sandwiched between FM insulators that allow magnon propagation thus the generation of magnon spin current by thermal gradient. Here, we report a new species of 2DEGs at oxide interfaces, which favors an efficient spin-to-charge conversion but does not need electron transmission and resonance spin pumping. By constructing the epitaxial heterostructure with FM EuO, which acts as a source for magnon spin current but is insulating for electric current, and dielectric $KTaO_3$ (KTO), spin current generated in EuO by thermal gradient has been directly injected into the 2DEG residing in the interfacial layer of KTO (Figure. 1a), yielding unbalanced electron momentum due to the IEE of the 2DEG and, thus, a sizable electric output (Figure 1b,c). Because spin injection takes place in the manner of thermal diffusion of non-equilibrium magnons rather than electron transmission through EuO, the impedance of the oxide insulator to spin current is avoided. Because spin injection is driven by temperature gradient, possible parasitic effects associated with FMR are eliminated.

2DEG at the EuO−KTO interface has been fabricated by epitaxially growing a EuO layer on (001)-oriented KTO single crystal substrate ($5 \times 3 \times 0.5$ mm^3) using a molecular beam epitaxy system with a base pressure below 2×10^{-10} mbar, following the procedures described in ref 23. Substrate temperature was set to 500 °C. In total, five samples were prepared with layer thicknesses of t = 5, 9, 15, 30, and 45 nm, respectively. A 2 nm thick MgO cap layer was in situ deposited to avoid the degrading of EuO in air. The technique of small-angle X-ray reflectivity has been adopted for the determination of layer thickness. X-ray diffraction indicates that the EuO layer thus obtained is single crystal, with its lattice rotating along [001] axis by 45° with respect to that of KTO to get epitaxial growth on KTO.[23]

As shown by the θ-2θ X-ray scan spectra in Figure 2a, the EuO layer exhibits clear (00l) reflections. A Φ-scan around the (111) peak of the EuO (001) film and the KTO (001)

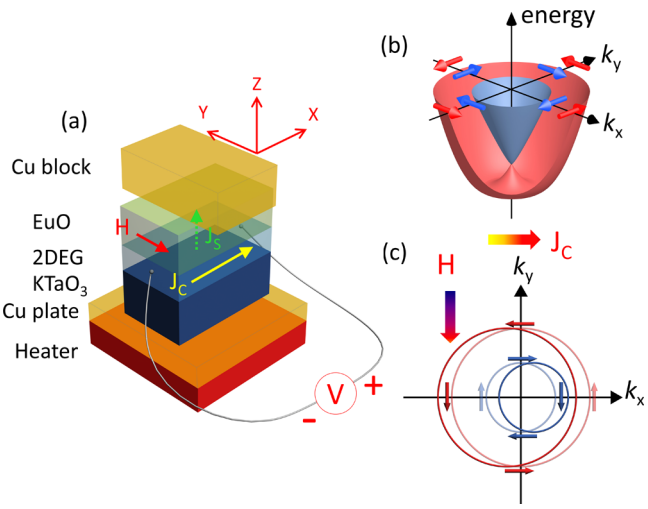

Figure 1. Sketches for thermal spin injection and the IEE of the EuO−$KTaO_3$ interface. (a) A schematic experiment setup for the investigation of spin Seebeck IEE. The directions of magnetic field, spin current, and electric measurement are mutually orthogonal. J_C and J_S denote the direction of charge current and magnon propagation, respectively. (b) Band structure for the Rashba-type two-dimensional electron system. Arrows mark the directions of electron spins. (c) Fermi contours at the Fermi level in equilibrium (light line) and non-equilibrium state (bold line). Thick arrows mark the directions of spin polarization and electric current, respectively. The left (right) shift of the outer (inner) Fermi contour is due to spin accumulation. In the case of thermal spin injection, J_S points to the direction of magnon propagation. These magnons have a spin polarization opposite to applied field because they are excited spin waves. In contrast, the spin polarization of the injected magnons into 2DEG aligns along the field direction. To focus on the main feature of the spin Seebeck IEE, possible distortions in spin textures due to the spin polarization of the 2DEG have been ignored.

substrate indicates that the EuO layer is epitaxial, consistent with the result of reflected high-energy electron diffraction.[23]

The EuO−KTO interface is highly metallic. As shown in Figure 2b, sheet resistance (R_S) displays a rapid decrease upon cooling. This behavior is observed in all samples. The R_S(300 K)/R_S(2 K) ratio is around 5.5. The decrease in the layer thickness of EuO generally causes a slight upward shift of the entire R_S−T curve but does not affect the metallic character of the interface, where T represents temperature. A further analysis yields a rectify-shaped anisotropic magnetoresistance,[23] indicating that the conduction of the EuO−KTO interface is indeed two-dimensional in nature. The deduced layer thickness of the 2DEG is about 6 nm.[23]

As is well-documented,[24−26] Eu atoms deposited in ultrahigh vacuum will uptake oxygen atoms from the surface layer of oxide substrate to form the EuO phase, leaving behind oxygen vacancies. For the KTO substrate, when the content of oxygen vacancies is high enough, a metallic 2DEG will appear, residing in an interfacial layer. The layer thickness of EuO slightly influences sheet resistance by affecting the outward oxygen diffusion from KTO thus the carrier density of 2DEG. A direct measurement of Hall resistance shows that the carrier density grows from ~1.0×10^{14} to 1.2×10^{14} cm^{-2} as the layer thickness increases from 5 to 15 nm (T = 10 K), while the corresponding mobility changes from ~82 to ~101 cm^2/(V s) (see Figure S1). Even a thick EuO layer causes a slight decrease in mobility, probably due to interlayer atomic diffusion.

DOI: 10.1021/acs.nanolett.8b04509
Nano Lett. 2019, 19, 1605−1612

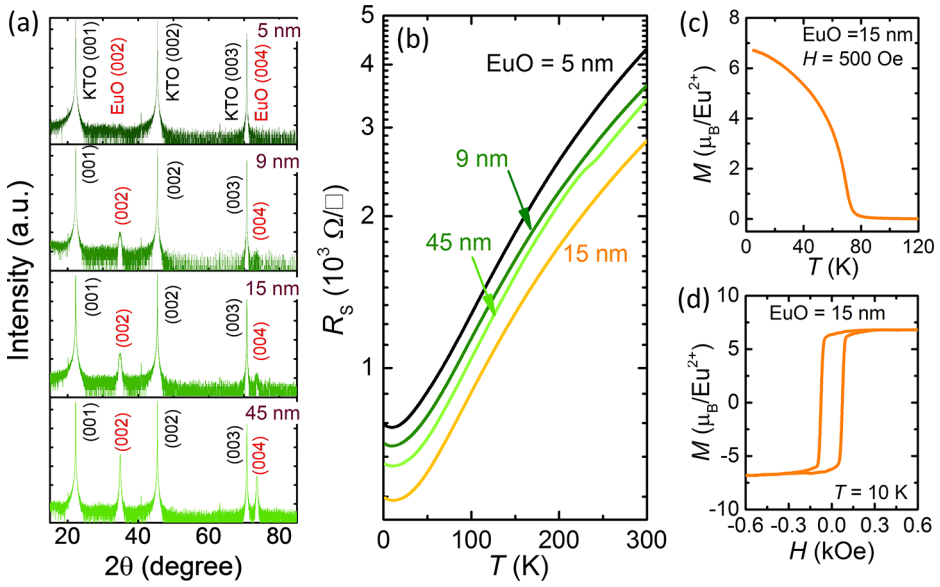

Figure 2. Structural, transport, and magnetic properties of the EuO/KTO heterostructures. (a) X-ray diffraction spectra of the samples with different EuO layer thicknesses. (00*l*) reflections of the EuO layer can be clearly seen. Here, the intensity of the (002) reflection of KTO has been normalized to the same value for comparison. (b) Sheet resistance as a function of temperature for different 2DEGs, showing the typical metallic behaviors. (c) Thermomagnetic curve measured under a magnetic field of 0.05 T in field-cooling mode for the sample of t = 15 nm. FM order sets in around 70 K. (d) A magnetic loop of the EuO layer, obtained at 10 K with in-plane magnetic field for the same sample of panel c. It indicates an easy-plane axis.

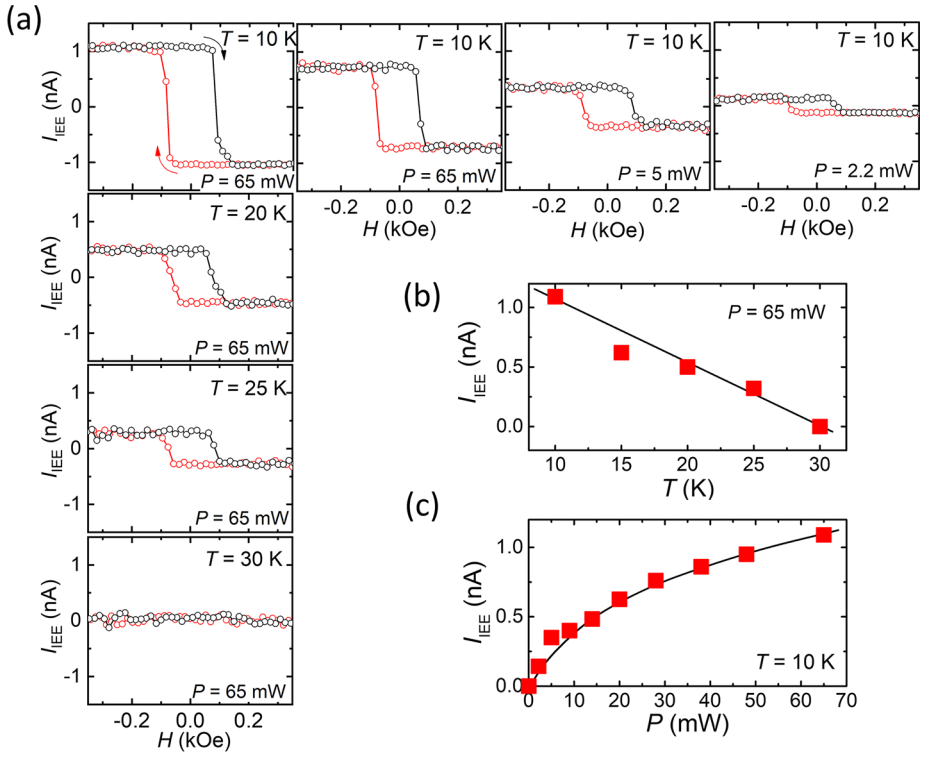

Figure 3. Spin Seebeck IEE of a EuO−KTO interface with the EuO layer thickness of 15 nm. (a) Left column: magnetic-field dependence of thermoelectric current measured under a fixed heating power of P = 65 mW but different temperatures. Horizontal row: magnetic-field dependence of thermoelectric current measured under a fixed temperature of 10 K but different heating powers. (b) Thermoelectric current as a function of temperature. P = 65 mW. (c) Thermoelectric current as a function of heating power, obtained at 10 K. Arrows in the figure mark the direction of magnetic cycling. Here, heating power instead of ΔT was adopted because of the difficulty of getting an accurate ΔT when P is low.

EuO layers exhibit the standard FM behavior of the EuO phase. Figure 2c shows the temperature dependence of the magnetization (M) of a representative sample (t = 15 nm), measured with a field of H = 0.05 T in field-cooling mode. The typical magnetic transition is observed around T_C = 70 K. Figure 2d is the corresponding magnetic loop measured at 10 K along the film plane, in which magnetic easy axis lies. The saturation magnetization is very close to theoretical value (6.8

DOI: 10.1021/acs.nanolett.8b04509
Nano Lett. 2019, 19, 1605−1612

versus 7 μ_B/Eu^{2+}). These are the standard magnetic behaviors of the EuO phase. Variation in EuO layer thickness slightly influences the $M-T$ and $M-H$ relations, whereas the main magnetic characters of EuO remain unaffected (see Figure S2).

Spin Seebeck measurements were performed by a Quantum-designed physical property measurement system (PPMS). A Cu block (10 mm × 10 mm × 5 mm) was placed on the topside of the sample as a cold reservoir. To stabilize the temperature of sample surface, the cold sink was thermally contacted to the sample chamber of the PPMS. To be uniformly heated, the sample (5 mm × 3 mm × 0.5 mm) was mounted on a Cu plate (5 mm × 5 mm × 1 mm) under which a resistance heater located. To get good thermal contact, thermal adhesive was employed between Cu block (Cu plate) and sample. The whole package, including the top cold sink, the sample, and the bottom heating unit was mounted on a polyvinyl chloride sample holder. The temperature difference of the topside and backside of EuO/KTO was obtained by directly measuring the temperatures of the Cu cold sink and Cu plate via two thermocouples (Pt100 thermocouple with an area of 2 mm × 2 mm and a thickness of 0.2 mm). To generate non-equilibrium magnons in EuO, a thermal gradient is established by heating the backside Cu plate while keeping the cold sink at the preset temperature. Electric output (V_{IEE}) were collected, by a nanovoltmeter (Keithley 2182A), from two electrodes connected to 2DEG as the magnetic field is cycling between ±0.5 T along the interface (electrode separation of 4 mm). The left column of Figure 3a presents the magnetic-field dependence of the thermoelectric current I_{IEE} for the typical sample of t = 15 nm, measured at different temperatures under a fixed thermal gradient of $\nabla T \approx 18.8$ K/cm in the EuO layer (corresponding to a heating power of P = 65 mW). Here, I_{IEE} is defined by V_{IEE}/R. $R = R_S \times L/W$, with R_S being the square resistance of the 2DEG and L and W being electrode separation and sample width, respectively. The temperature difference between the backside and topside of EuO/KTO is 3.5 K, obtained by direct measurements. Adopting the thermal conductivity of ∼23.8 W/mK for EuO[27] and ∼6.3 W/mK for KTO[28] at 10 K, it is easy to estimate the thermal gradient in EuO. Corresponding to the negative to positive sweeping of the magnetic field, the thermoelectric current first takes a constant positive value and then, when H exceeds a threshold field, suddenly drops to a negative value that is the same as the positive one in magnitude. Reversing sweeping direction, an opposite process takes place at a negative threshold field. Finally, a rectangle-shaped clockwise $I_{IEE}-H$ loop is formed. Here the conventional thermopower stemming from longitudinal temperature gradient has been corrected, which is independent of magnetic field. Due to the presence of a Cu plate, the sample has been uniformly heated. The conventional thermopower caused by inhomogeneous heating, which results in an upward and downward shift of the whole $V_{IEE}-H$ loop, is smaller than 0.25 μV, only ∼25% of the spin Seebeck V_{IEE} (see Figure S3). Obviously, a vertical thermal gradient indeed generates a horizontal electric field in 2DEG in the presence of an orthogonal magnetic field, and the maximal thermoelectric current is ∼1.1 nA. Noting the fact that the electric current is negative (positive) when the magnetic moment of EuO aligns along (against) the field direction marked in Figure 1a, the electric field in 2DEG must direct along the yellow arrow, as shown in Figure 1a.

Notably, V_{IEE} changes its sign at a definite field of ±80 Oe, which is exactly the coercive field of EuO (Figure 2d). This result indicates that the sign change takes place accompanying the magnetization reversal of the EuO layer. This kind of phenomenon is usually observed when the sample exhibits an anomalous Nernst effect or a spin Seebeck effect. It cannot be the anomalous Nernst effect of the EuO layer because EuO is an insulator without mobile charges (see Figure S4). It cannot be the anomalous Nernst effect of the 2DEG either although 2DEG is magnetic[23] because the $V_{IEE}-H$ loop, in that case, should be counterclockwise on the analogy of the anomalous Hall effect of the 2DEG (see Figure S5); generally, the anomalous Nernst effect is equivalent to anomalous Hall effect except that the driving force for electric current now is thermal gradient rather than electric field. From first glance, the $V_{IEE}-H$ dependence here is similar to that resulted by spin Seebeck effect in the hybrid structure like Pt/YIG ($Y_3Fe_5O_{12}$) if EuO acts as YIG and 2DEG acts as Pt. As is well-documented,[29−32] when a temperature gradient is established in an insulating FM material, a thermal diffusion of non-equilibrium magnons will appear parallel to thermal gradient. This analysis implies the formation of a spin current in EuO and the spin injection to the EuO−KTO interface or 2DEG. Due to the Rashba spin-momentum locking of the 2DEG,[33] the spin accumulation will result in uncompensated electron momentums at the Fermi contours as sketched by Figure 1c, yielding an electric output. Based on these analyses, we can safely say that the spin-charge conversion here has been driven by the spin Seebeck IEE of the 2DEG.

To confirm this conclusion, we checked the current direction produced by the IEE. Because the sample is heated on backside, as shown in Figure 1a, the spin current will start from conducting interface and ending on the EuO surface.[34] This will cause a left (right) shift of the outer (inner) Fermi contour when the magnetization of EuO aligns along the downward direction as experimentally set (Figure 1c). As a consequence, the electron momentum is greater along than against the x axis. This implies an electron drift against the x axis, consistent with the experimental observation. Because the spin polarization of the spin current is parallel to the magnetic direction of the EuO layer, magnetization reversal thus reverses the direction of the electric output. As expected, when aligning spin polarization of spin current to the direction of electric measurement, V_{IEE} will vanish. In this case, uncompensated electron momentums appear in the perpendicular direction of electric measurements. Indeed, no V_{IEE} is detected after rotating magnetic field in film plane by 90° (see Figure S6).

As shown by the left column of Figure 3a, the spin Seebeck IEE is strongly temperature dependent. It is the strongest at 10 K and invisible at 30 K. We did not perform the experiments in the temperature range below 10 K because it is difficult to get a thermally stable state there. In general, the weakening of the IEE implies a reduction of the numbers of non-equilibrium magnons that reach the 2DEG. This effect could be ascribed to the decrease of the magnon lifetime at lifted temperatures[35] due to enhanced magnon−magnon or magnon−phonon interaction. Remarkably, the IEE disappears at a critical temperature that is well below of the Curie temperature of EuO (30 versus 70 K). This is consistent with a previous report that the EuO-induced magnetic hysteresis disappears above 30 K for the 2DEG at the EuO−KTO interface.[23] A possible explanation is that the interfacial layer of EuO has a lower Curie temperature. This will occur if Eu uptakes excessive oxygen atoms from KTO, forming the $EuO_{1+\delta}$ phase.[36,37] Figure 3b is a summary of the spin Seebeck IEE

DOI: 10.1021/acs.nanolett.8b04509
Nano Lett. 2019, 19, 1605−1612

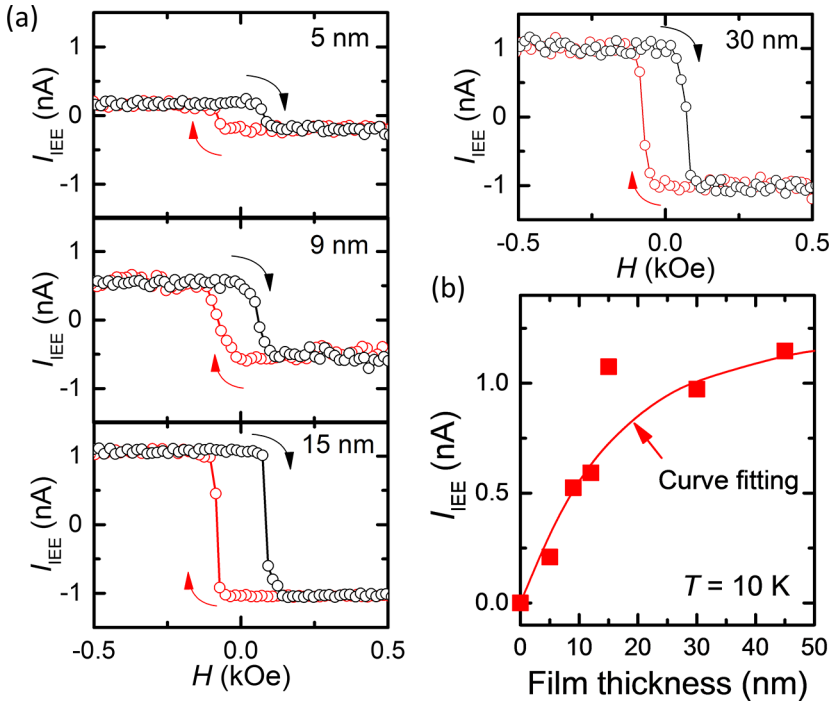

Figure 4. Comparison of the spin Seebeck IEE of different samples. (a) Magnetic-field dependence of thermoelectric current for different samples, measured at 10 K with a ∇T of 18.8 K/cm (P = 65 mW). The nominal thickness of the EuO is t = 5, 9, 15, and 30 nm. Arrows in the figure mark the direction of magnetic cycling. (b) Thermoelectric current as a function of layer thickness. A nearly linear growth of I_{IEE} in the initially stage and a tendency toward saturation above the layer thickness of 30 nm can be clearly seen. The solid line is the result of curve fitting to the equation of $I_{IEE} = I_{IEE0}[1 - \exp(-t/\lambda)]$, which reveals the influence of finite magnon propagation length on I_{IEE}.

voltages obtained at different temperatures. V_{IEE}, which is defined by $[V_{IEE}(-0.3\ \text{kOe}) - V_{IEE}(+0.3\ \text{kOe})]/2$, is ~1 μV at 10 K. The corresponding current is 1.1 nA. With the increase of temperature, the thermoelectric current linearly decreases and vanishes above 30 K.

The horizontal row in Figure 3a depicts the I_{IEE}–H loop as a function of heating power, obtained at a fixed temperature of 10 K. As expected, I_{IEE} is zero without being heated (not shown), i.e., thermal gradient is indispensable for the spin Seebeck IEE. I_{IEE} is ~0.1 nA when the heating power is 2.2 mW and ~1.1 nA when P is 65 mW, monotonically increasing with heating power. This is understandable because a higher heating power will generate a greater thermal gradient thus a stronger spin current. The I_{IEE}–P relation is depicted in Figure 3c. I_{IEE} increases rapidly as P starts to grow from zero and tends to a state of saturation when P exceeds 40 mW. The nonlinear relation means the enhancement of energy dissipation when heating power is high.

To get further information on spin Seebeck IEE, we performed a systematic investigation of the samples with different EuO layer thicknesses. As shown in Figure 4a, the V_{IEE}-H loop varies from sample to sample. The I_{IEE} step at the threshold magnetic field displays an obvious increase with t. It is ~0.2 nA for t = 5 nm and ~1.0 nA for t = 30 nm, enhancing by a factor up to 5 as t increases. The magnetic behaviors of these samples are similar and, thus, are unlikely to be responsible for the different thermoelectric effects (see Figure S2). Considering the fact that thick EuO layers can provide more non-equilibrium magnons, the spin current received by the 2DEG will increase with film thickness. In this picture, we can understand the strong thickness dependence of I_{IEE}. At first glance, however, the I_{IEE} growth with t is nonlinear, slowing down when the film is thick. This means a reduction of the contributions to the I_{IEE} of the distant magnons from interface due to the finite propagation length.

Depicting the thermoelectric current as a function of layer thickness, we obtained a quantitative relationship between I_{IEE} and t. As shown in Figure 4b, I_{IEE} increases nearly linearly with film thickness in the initial stage. This behavior is expected to appear when the film thickness is shorter than magnon propagation length. In this case, the number of non-equilibrium magnons collected by the EuO–KTO interface will be proportional to film thickness. Notably, strong thickness dependence of the spin Seebeck effect has already been reported for the Pt/YIG hybrid structures.[35,38] When t is thick enough, however, the growth speed of I_{IEE} with t slows down, exhibiting a tendency toward saturation. This behavior will appear when the film thickness is greater than the magnon diffusion distance. In this case, distant non-equilibrium magnons annihilate on their way toward the 2DEG. According to Kehlberger et al.,[38] there will be a simple relation $I_{IEE} = I_{IEE0}[1 - \exp(-t/\lambda)]$ if the I_{IEE}–t dependence is determined by the magnon diffusion, where I_{IEE0} and λ are two adjustable parameters, with λ being magnon propagation length. Indeed, the experimental data in Figure 4b can be well-described by the above equation adopting the fitting parameters of I_{IEE0} = 1.2 nA and λ = 16 nm. Obviously, it is the near interface layer of EuO that dominates the spin Seebeck effect. Magnons more than 16 nm away from interface have a very low probability to be collected by interface thus have negligible contributions. Remarkably, the magnon propagation length deduced here (16 nm) is much smaller than that of YIG (~10 μm) but comparable to that reported for γ-Fe_2O_3[39] and Fe_3O_4.[40] Short magnon diffusion distance could be a general feature of most magnetic oxides.

DOI: 10.1021/acs.nanolett.8b04509
Nano Lett. 2019, 19, 1605–1612

Unlike the case of spin pumping by FMR, it is not possible to determine the efficiency or the Rashba−Edelstein parameter for the spin-charge conversion in the case of thermal spin injection, due to the difficulty to estimate spin current. To quantify thermoelectric efficiency, we define a spin Seebeck coefficient by SSC = $E_{IEE}/\nabla T$, where E_{IEE} equals V_{IEE}/L with L being the electrode separation for voltage measurements. Actually, SSC is the electric field produced by unit temperature gradient via spin Seebeck effect. It thus allows a comparison of the thermoelectric efficiency of different systems. In Figure 5,

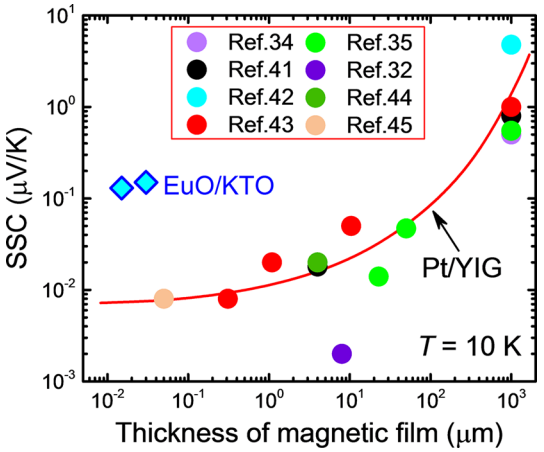

Figure 5. Spin Seebeck coefficient as a function of the thickness of magnetic layer for the EuO/KTO (diamonds) and Pt/YIG (solid circles) hybrid structures, depicted at a fixed temperature of 10 K. The data of Pt/YIG have been collected from the literature denoted in the figure. The Pt films have the thicknesses between 5 and 10 nm. The solid line is a guide for the eye.

we show the SSC values of EuO/KTO for two selected film thicknesses of t = 15 and 45 nm. The corresponding results are ∼0.13 and ∼0.15 μV/K. For comparison, the reported SSC values for the Pt/YIG hybrid structures are also presented in Figure 5, with the YIG layer thickness ranging from 50 nm to 1 mm. Pt/YIG is a model system for the investigation of spin Seebeck effect. YIG owns the longest magnon diffusion distance among magnetic materials (∼10 μm) and Pt has a strong spin−orbit interaction. According to Figure 5, SSC is around 1 μV/K when the thickness of the YIG slab is 1 mm, which is larger by a factor of 6.7 than the SSC of EuO/KTO. This is understandable. Because of the long magnon propagation distance, thicker YIG slabs will provide more effective non-equilibrium magnons for the Pt detector. With the decrease of film thickness, however, SSC undergoes a rapid decrease. It is ∼0.02 μV/K when t = 1 μm and ∼0.008 μV/K when t = 50 nm. Comparing the results for the EuO/KTO and Pt/YIG heterostructures with the same thickness for magnetic layer (∼50 nm), the SSC of the former system is greater by a factor of ∼19 than that of the latter. Obviously, the EuO/KTO system is much more efficient than Pt/YIG for thermoelectric conversion.

Here, we emphasize that the spin current in EuO/KTO appears accompanying the diffusion of non-equilibrium magnons and is directly injected into the 2DEG at the oxide interface. This is different from the FM film/LAO/STO system, for which the spin injection to 2DEG is achieved by transmitting electrons through the LAO layer and, thus, is strongly depressed at low temperatures.[16] The efficiency of thermal spin injection cannot be directly compared to that of spin pumping by FMR. As an alternative, we studied the effect of an insulating buffer layer on the spin Seebeck IEE. A control sample has been fabricated for this investigation, which is composed of EuO (15 nm), KTO and an intermediate $LaTiO_3$ layer (5 unit cells in thickness). It is found that V_{IEE} is ∼1 μV for EuO/KTO and ∼25 nV for EuO/$LaTiO_3$/KTO for a fixed thermal gradient of 18.8 K/cm (see Figure S7). The $LaTiO_3$ layer has severely depressed the thermoelectric effect. Obviously, $LaTiO_3$ has blocked the spin current transmission from EuO to 2DEG. Here, $LaTiO_3$ rather than $LaAlO_3$ was adopted as buffer layer because $LaAlO_3$ always forms an amorphous layer when deposited on KTO, even at high temperatures.[46]

The 5d oxide KTO is distinct due to its strong spin−orbit coupling. The electronic structure of the 2DEG residing in KTO is therefore especially attractive. Based on the measurement of angle-resolved photoemission (ARPES), King et al.[47] obtained the sub-band structure of the 2DEG yielded by irradiating KTO surface, which has been cleaved in an ultrahigh vacuum, using UV light. Unfortunately, the Rashba spin splitting of the 2DGE cannot be resolved from the ARPES spectrum. Based on the analysis of the effect of weak anti-localization for the 2DEG at the amorphous LAO−KTO interface, Zhang et al.[48] obtained the Rashba coupling constant of ∼0.1 eV Å. This constant is comparable to the topological insulator, which is known for its strong spin−orbit interaction (∼0.36 eV Å for Bi_2Se_3[49]). Therefore, large Rashba spin splitting and direct spin injection both cause the strong spin Seebeck IEE observed here.

In conclusion, 2DEGs sandwiched between ferromagnetic insulators EuO and 5d oxides $KTaO_3$ have been obtained. A direct thermal spin injection from EuO to 2DEG and an efficient spin-to-charge conversion have been achieved via the inverse Edelstein effect of the conducting interface. The propagation length of non-equilibrium magnons in EuO has been determined. The present work suggests a potential application of magnetic 2DEGs to spintronics.

■ ASSOCIATED CONTENT

Supporting Information

The Supporting Information is available free of charge on the ACS Publications website at DOI: 10.1021/acs.nanolett.8b04509.

Figures showing the temperature dependence of carrier density and mobility, magnetic behaviors, current−voltage curves, thermoelectric voltage measured with the magnetic field applied along two orthogonal in-plane directions, and related analysis regarding the anomalous Nernst effect (PDF)

■ AUTHOR INFORMATION

Corresponding Author

*E-mail: jrsun@iphy.ac.cn.

ORCID

Xiaobing Chen: 0000-0003-4327-1209
Shuanhu Wang: 0000-0002-5386-1037
Wei Han: 0000-0002-1757-4479
Jirong Sun: 0000-0003-1238-8770

Notes

The authors declare no competing financial interest.

DOI: 10.1021/acs.nanolett.8b04509
Nano Lett. 2019, 19, 1605−1612

■ ACKNOWLEDGMENTS

This work has been supported by the National Basic Research of China (grant nos. 2016YFA0300701, 2018YFA0305704, 2015CB921104, and 2017YFA0206300), the National Natural Science Foundation of China (grant nos. 11520101002, 11574006, 51590880, 51531008, and 11604265), and the Key Program of the Chinese Academy of Sciences.

■ REFERENCES

(1) Bert, J. A.; Kalisky, B.; Bell, C.; Kim, M.; Hikita, Y.; Hwang, H. Y.; Moler, K. A. Direct imaging of the coexistence of ferromagnetism and superconductivity at the $LaAlO_3/SrTiO_3$ interface. *Nat. Phys.* **2011**, *7*, 767−771.

(2) Li, L.; Richter, C.; Mannhart, J.; Ashoori, R. C. Coexistence of magnetic order and two-dimensional superconductivity at $LaAlO_3/SrTiO_3$ interfaces. *Nat. Phys.* **2011**, *7*, 762−766.

(3) Dikin, D. A.; Mehta, M.; Bark, C. W.; Folkman, C. M.; Eom, C. B.; Chandrasekhar, V. Coexistence of Superconductivity and Ferromagnetism in Two Dimensions. *Phys. Rev. Lett.* **2011**, *107*, 056802.

(4) Stornaiuolo, D.; Cantoni, C.; De Luca, G. M.; Di Capua, R.; Di Gennaro, E.; Ghiringhelli, G.; Jouault, B.; Marre, D.; Massarotti, D.; Miletto Granozio, F.; Pallecchi, I.; Piamonteze, C.; Rusponi, S.; Tafuri, F.; Salluzzo, M. Tunable spin polarization and superconductivity in engineered oxide interfaces. *Nat. Mater.* **2016**, *15*, 278−283.

(5) Gardner, H. J.; Kumar, A.; Yu, L. Q.; Xiong, P.; Warusawithana, M. P.; Wang, L. Y.; Vafek, O.; Schlom, D. G. Enhancement of superconductivity by a parallelmagnetic field in two-dimensional superconductors. *Nat. Phys.* **2011**, *7*, 895−900.

(6) Pallecchi, I.; Telesio, F.; Li, D.; Fête, A.; Gariglio, S.; Triscone, J. M.; Filippetti, A.; Delugas, P.; Fiorentini, V.; Marre, D. Giant oscillating thermopower at oxide interfaces. *Nat. Commun.* **2015**, *6*, 6678.

(7) Narayanapillai, K.; Gopinadhan, K.; Qiu, X. P.; Annadi, A.; Yang, H.; Venkatesan, T. Current-driven spin orbit field in $LaAlO_3/SrTiO_3$ heterostructures. *Appl. Phys. Lett.* **2014**, *105*, 162405.

(8) He, P.; Walker, S. M.; Zhang, S. S.-L.; Bruno, F. Y.; Bahramy, M. S.; Lee, J. M.; Ramaswamy, R.; Cai, K. M.; Heinonen, O.; Vignale, G.; Baumberger, F.; Yang, H. Observation of out-of-plane spin texture in a $SrTiO_3(111)$ two-dimensional electron gas. *Phys. Rev. Lett.* **2018**, *120*, 266802.

(9) Thiel, S.; Hammerl, G.; Schmehl, A.; Schneider, C. W.; Mannhart, J. Tunable Quasi-Two-Dimensional Electron Gases in Oxide Heterostructures. *Science* **2006**, *313*, 1942−1945.

(10) Edelstein, V. M. Spin polarization of conduction electrons induced by electric current in two-dimensional asymmetric electron systems. *Solid State Commun.* **1990**, *73*, 233−235.

(11) Rojas Sánchez, J.-C.; Vila, L.; Desfonds, G.; Gambarelli, S.; Attané, J. P.; De Teresa, J. M.; Magén, C.; Fert, A. Spin-to-charge conversion using Rashba coupling at the interface between non-magnetic materials. *Nat. Commun.* **2013**, *4*, 2944.

(12) Zhang, W.; Jungfleisch, M. B.; Jiang, W.; Pearson, J. E.; Hoffmann, A. Spin pumping and inverse Rashba-Edelstein effect in NiFe/Ag/Bi and NiFe/Ag/Sb. *J. Appl. Phys.* **2015**, *117*, 17C727.

(13) Rojas-Sánchez, J.-C.; Oyarzún, S.; Fu, Y.; Marty, A.; Vergnaud, C.; Gambarelli, S.; Vila, L.; Jamet, M.; Ohtsubo, Y.; Taleb-Ibrahimi, A.; Le Fèvre, P.; Bertran, F.; Reyren, N.; George, J.-M.; Fert, A. Spin to Charge Conversion at Room Temperature by Spin Pumping into a New Type of Topological Insulator: α-Sn Films. *Phys. Rev. Lett.* **2016**, *116*, 096602.

(14) Shiomi, Y.; Nomura, K.; Kajiwara, Y.; Eto, K.; Novak, M.; Segawa, K.; Ando, Y.; Saitoh, E. Spin-Electricity Conversion Induced by Spin Injection into Topological Insulators. *Phys. Rev. Lett.* **2014**, *113*, 196601.

(15) Lesne, E.; Fu, Y.; Oyarzun, S.; Rojas-Sanchez, J. C.; Vaz, D. C.; Naganuma, H.; Sicoli, G.; Attane, J. P.; Jamet, M.; Jacquet, E.; George, J.-M.; Barthélémy, A.; Jaffrès, H.; Fert, A.; Bibes, M.; Vila, L. Highly efficient and tunable spin-to-charge conversion through Rashba coupling at oxide interfaces. *Nat. Mater.* **2016**, *15*, 1261−1266.

(16) Song, Q.; Zhang, H. R.; Su, T.; Yuan, W.; Chen, Y. Y.; Xing, W. Y.; Shi, J.; Sun, J. R.; Han, W. Observation of inverse Edelstein effect in Rashba-split 2DEG between $SrTiO_3$ and $LaAlO_3$ at room temperature. *Sci. Adv.* **2017**, *3*, e1602312.

(17) Wang, Y.; Ramaswamy, R.; Motapothula, M.; Narayanapillai, K.; Zhu, D.; Yu, J.; Venkatesan, T.; Yang, H. Room-Temperature Giant Charge-to-Spin Conversion at the $SrTiO_3−LaAlO_3$ Oxide Interface. *Nano Lett.* **2017**, *17*, 7659−7664.

(18) Egan, W. G.; Juretschke, H. J. DC Detection of Ferromagnetic Resonance in Thin Nickel Films. *J. Appl. Phys.* **1963**, *34*, 1477−1484.

(19) Harder, M.; Gui, Y.; Hu, C.-M. Electrical detection of magnetization dynamics via spin rectification effects. *Phys. Rep.* **2016**, *661*, 1−59.

(20) Iguchi, R.; Saitoh, E. Measurement of Spin Pumping Voltage Separated from Extrinsic Microwave Effects. *J. Phys. Soc. Jpn.* **2017**, *86*, 011003.

(21) Keller, S.; Greser, J.; Schweizer, M. R.; Conca, A.; Lauer, V.; Dubs, C.; Hillebrands, B.; Papaioannou, E. Th. Relative weight of the inverse spin-Hall and spin-rectification effects for metallic polycrystalline Py/Pt, epitaxial Fe/Pt, and insulating YIG/Pt bilayers: Angular dependent spin pumping measurements. *Phys. Rev. B: Condens. Matter Mater. Phys.* **2017**, *96*, 024437.

(22) Yue, D.; Lin, W.; Li, J.; Jin, X.; Chien, C. L. Spin-to-Charge Conversion in Bi Films and Bi/Ag Bilayers. *Phys. Rev. Lett.* **2018**, *121*, 037201.

(23) Zhang, H. R.; Yun, Y.; Zhang, X. J.; Zhang, H.; Ma, Y.; Yan, X.; Wang, F.; Li, G.; Li, R.; Khan, T.; Chen, Y. S.; Liu, W.; Hu, F. X.; Liu, B. G.; Shen, B. G.; Han, W.; Sun, J. R. High-Mobility Spin-Polarized Two-Dimensional Electron Gases at $EuO/KTaO_3$ Interfaces. *Phys. Rev. Lett.* **2018**, *121*, 116803.

(24) Sutarto, R.; Altendorf, S. G.; Coloru, B.; Moretti Sala, M.; Haupricht, T.; Chang, C. F.; Tjeng, L. H.; Hu, Z.; Hollmann, N.; Kierspel, H.; et al. Epitaxial and layer-by-layer growth of EuO thin films on yttria-stabilized cubic zirconia (001) using MBE distillation. *Phys. Rev. B: Condens. Matter Mater. Phys.* **2009**, *79*, 205318.

(25) Lömker, P.; Rödel, T. C.; Gerber, T.; Fortuna, F.; Frantzeskakis, E.; Le Fèvre, P.; Bertran, F.; Müller, M.; Santander-Syro, A. F. Two-dimensional electron system at the magnetically tunable $EuO/SrTiO_3$ interface. *Phys. Rev. Mater.* **2017**, *1*, No. 062001.

(26) Yun, Y.; Ma, Y.; Su, T.; Xing, W. Y.; Chen, Y. Y.; Yao, Y. Y.; Cai, R. R.; Yuan, W.; Han, W. Role of La doping for topological Hall effect in epitaxial EuO films. *Phys. Rev. Mater.* **2018**, *2*, 034201.

(27) Martin, J. J.; Dixon, G. S. Thermal transport in EuO. *Phys. Status Solidi B* **1972**, *54*, 707−712.

(28) Tachibana, M.; Kolodiazhnyi, T.; Takayama-Muromachi, E. Thermal conductivity of perovskite ferroelectrics. *Appl. Phys. Lett.* **2008**, *93*, 092902.

(29) Uchida, K.; Adachi, H.; Ota, T.; Nakayama, H.; Maekawa, S.; Saitoh, E. Observation of longitudinal spin-Seebeck effect in magnetic insulators. *Appl. Phys. Lett.* **2010**, *97*, 172505.

(30) Uchida, K.; Ishida, M.; Kikkawa, T.; Kirihara, A.; Murakami, T.; Saitoh, E. Longitudinal spin Seebeck effect: from fundamentals to applications. *J. Phys.: Condens. Matter* **2014**, *26*, 343202.

(31) Schreier, M.; Kamra, A.; Weiler, M.; Xiao, J.; Bauer, G. E. W.; Gross, R.; Goennenwein, S. T. B. Magnon, phonon, and electron temperature profiles and the spin Seebeck effect in magnetic insulator/normal metal hybrid structures. *Phys. Rev. B: Condens. Matter Mater. Phys.* **2013**, *88*, 094410.

(32) Rezende, S. M.; Rodríguez-Suárez, R. L.; Cunha, R. O.; Rodrigues, A. R.; Machado, F. L. A.; Fonseca Guerra, G. A.; Lopez Ortiz, J. C.; Azevedo, A. Magnon spin-current theory for the longitudinal spin-Seebeck effect. *Phys. Rev. B: Condens. Matter Mater. Phys.* **2014**, *89*, 014416.

(33) Manchon, A.; Koo, H. C.; Nitta, J.; Frolov, S. M.; Duine, R. A. New perspectives for Rashba spin−orbit coupling. *Nat. Mater.* **2015**, *14*, 871−882.

DOI: 10.1021/acs.nanolett.8b04509
Nano Lett. 2019, 19, 1605−1612

(34) Kikkawa, T.; Uchida, K.; Daimon, S.; Saitoh, E. Complete suppression of longitudinal spin Seebeck effect by frozen magnetization dynamics in $Y_3Fe_5O_{12}$. *J. Phys. Soc. Jpn.* **2016**, *85*, 065003.
(35) Guo, E. J.; Cramer, J.; Kehlberger, A.; Ferguson, C. A.; MacLaren, D. A.; Jakob, G.; Kläui, M. Influence of thickness and interface on the low-temperature enhancement of the spin Seebeck effect in YIG films. *Phys. Rev. X* **2016**, *6*, 031012.
(36) Holmes, L.; Schieber, M. M. Metamagnetism in Eu_3O_4. *Phys. Rev.* **1968**, *167*, 449−457.
(37) Mairoser, T.; Mundy, J. A.; Melville, A.; Hodash, D.; Cueva, P.; Held, R.; Glavic, A.; Schubert, J.; Muller, D. A.; Schlom, D. G.; Schmehl, A. High-quality EuO thin films the easy way via topotactic transformation. *Nat. Commun.* **2015**, *6*, 7716.
(38) Kehlberger, A.; Ritzmann, U.; Hinzke, D.; Guo, E. J.; Cramer, J.; Jakob, G.; Onbasli, M. C.; Kim, D. H.; Ross, C. A.; Jungfleisch, M. B.; Hillebrands, B.; Nowak, U.; Kläui, M. Length scale of the spin Seebeck effect. *Phys. Rev. Lett.* **2015**, *115*, 096602.
(39) Jiménez-Cavero, P.; Lucas, I.; Anadón, A.; Ramos, R.; Niizeki, T.; Aguirre, M. H.; Algarabel, P. A.; Uchida, K.; Ibarra, M. R.; Saitoh, E.; Morellón, L. Spin Seebeck effect in insulating epitaxial γ−Fe_2O_3 thin films. *APL Mater.* **2017**, *5*, 026103.
(40) Anadón, A.; Ramos, R.; Lucas, I.; Algarabel, P. A.; Morellón, L.; Ibarra, M. R.; Aguirre, M. H. Characteristic length scale of the magnon accumulation in Fe_3O_4/Pt bilayer structures by incoherent thermal excitation. *Appl. Phys. Lett.* **2016**, *109*, 012404.
(41) Jin, H.; Boona, S. R.; Yang, Z. H.; Myers, R. C.; Heremans, J. P. Effect of the magnon dispersion on the longitudinal spin Seebeck effect in yttrium iron garnets. *Phys. Rev. B: Condens. Matter Mater. Phys.* **2015**, *92*, 054436.
(42) Iguchi, R.; Uchida, K.; Daimon, S.; Saitoh, E. Concomitant enhancement of the longitudinal spin Seebeck effect and the thermal conductivity in a Pt/YIG/Pt system at low temperatures. *Phys. Rev. B: Condens. Matter Mater. Phys.* **2017**, *95*, 174401.
(43) Kikkawa, T.; Uchida, K.; Daimon, S.; Qiu, Z. Y.; Shiomi, Y.; Saitoh, E. Critical suppression of spin Seebeck effect by magnetic fields. *Phys. Rev. B: Condens. Matter Mater. Phys.* **2015**, *92*, 064413.
(44) Kikkawa, T.; Shen, K.; Flebus, B.; Duine, R. A.; Uchida, K.; Qiu, Z. Y.; Bauer, G. E. W.; Saitoh, E. Magnon polarons in the spin Seebeck effect. *Phys. Rev. Lett.* **2016**, *117*, 207203.
(45) Siegel, G.; Prestgard, M. C.; Teng, S.; Tiwari, A. Robust longitudinal spin-Seebeck effect in Bi-YIG thin films. *Sci. Rep.* **2015**, *4*, 4429.
(46) Zhang, H.; Zhang, H. R.; Yan, X.; Zhang, X. J.; Zhang, Q. H.; Zhang, J.; Han, F. R.; Gu, L.; Liu, B. G.; Chen, Y. S.; Shen, B. G.; Sun, J. R. Highly mobile two-dimensional electron gases with a strong gating effect at the amorphous $LaAlO_3/KTaO_3$ interface. *ACS Appl. Mater. Interfaces* **2017**, *9*, 36456−36461.
(47) King, P. D. C.; He, R. H.; Eknapakul, T.; Buaphet, P.; Mo, S.-K.; Kaneko, Y.; Harashima, S.; Hikita, Y.; Bahramy, M. S.; Bell, C.; Hussain, Z.; Tokura, Y.; Shen, Z.-X.; Hwang, H. Y.; Baumberger, F.; Meevasana, W. Subband structure of a two-dimensional electron gas formed at the polar surface of the strong spin-orbit perovskite $KTaO_3$. *Phys. Rev. Lett.* **2012**, *108*, 117602.
(48) Zhang, H.; Yan, X.; Zhang, X. J.; Wang, S.; Xiong, C. M.; Zhang, H. R.; Qi, S. J.; Zhang, J. E.; Han, F. R.; Wu, N.; Liu, B. G.; Chen, Y. S.; Shen, B. G.; Sun, J. R. Unusual electric and optical tuning of $KTaO_3$-based two-dimensional electron gases with 5d orbitals. *ACS Nano* **2019**, *13*, 609.
(49) King, P. D. C.; Hatch, R. C.; Bianchi, M.; Ovsyannikov, R.; Lupulescu, C.; Landolt, G.; Slomski, B.; Dil, J. H.; Guan, D.; Mi, J. L.; Rienks, E. D. L.; Fink, J.; Lindblad, A.; Svensson, S.; Bao, S.; Balakrishnan, G.; Iversen, B. B.; Osterwalder, J.; Eberhardt, W.; Baumberger, C.; Hofmann, Ph. Large tunable rashba spin splitting of a two-dimensional electron gas in Bi_2Se_3. *Phys. Rev. Lett.* **2011**, *107*, 096802.

NOTE ADDED AFTER ASAP PUBLICATION

This paper was published ASAP on February 11, 2019 with an error in Figure 3. The revised paper was published on February 14, 2019.

DOI: 10.1021/acs.nanolett.8b04509
Nano Lett. 2019, 19, 1605−1612